

LOCAL RADIATION MHD INSTABILITIES IN MAGNETICALLY STRATIFIED MEDIA

TED TAO AND OMER BLAES

Department of Physics, University of California, Santa Barbara CA 93106

ABSTRACT

We study local radiation magnetohydrodynamic instabilities in static, optically thick, vertically stratified media with constant flux mean opacity. We include the effects of vertical gradients in a horizontal background magnetic field. Assuming rapid radiative diffusion, we use the zero gas pressure limit as an entry point for investigating the coupling between the photon bubble instability and the Parker instability. Apart from factors that depend on wavenumber orientation, the Parker instability exists for wavelengths longer than a characteristic wavelength λ_{tran} , while photon bubbles exist for wavelengths shorter than λ_{tran} . The growth rate in the Parker regime is independent of the orientation of the horizontal component of the wavenumber when radiative diffusion is rapid, but the range of Parker-like wavenumbers is extended if there exists strong horizontal shear between field lines (i.e. horizontal wavenumber perpendicular to the magnetic field). Finite gas pressure introduces an additional short wavelength limit to the Parker-like behavior, and also limits the growth rate of the photon bubble instability to a constant value at short wavelengths. We also consider the effects of differential rotation with accretion disk applications in mind. Our results may explain why photon bubbles have not yet been observed in recent stratified shearing box accretion disk simulations. Photon bubbles may physically exist in simulations with high radiation to gas pressure ratios, but higher spatial resolution will be needed to resolve the asymptotically growing unstable wavelengths.

Subject headings: accretion, accretion disks — instabilities — MHD — radiative transfer

1. INTRODUCTION

Considerable attention has been devoted recently to the study of radiation pressure driven instabilities in magnetized media, which have generally come to be known as photon bubble instabilities. This name is particularly appropriate to the buoyant long wavelength instabilities studied by Arons (1992) in the context of accreting X-ray pulsars. Gammie (1998) found that an analogous instability is likely to exist in radiation-dominated accretion disks. Blaes & Socrates (2001, 2003) extended Gammie’s analysis to finite gas sound speeds and short wavelengths to show that the instability in this regime is a radiative amplification of magnetosonic modes. At least in media where Thomson scattering is the dominant opacity, the slow mode always has the fastest growth rate. Begelman (2001) derived a fully nonlinear periodic shock train solution to the equations of radiation MHD, which he suggested would be the nonlinear outcome of the short wavelength photon bubble instability. This was later confirmed by numerical simulation (Turner et al. 2005). Begelman (2006a) has also discovered a nonlinear wave solution in the long wavelength, buoyancy regime of the photon bubble instability.

Applications of the short wavelength photon bubble instability to accretion disks have been explored extensively by Begelman (2002, 2006b). Perhaps the most significant implication is that the instability might permit highly super-Eddington luminosities from accretion disks that would still be geometrically thin in terms of their vertical mass distribution. The physics of the short wavelength photon bubble instability has also been extended to situations where other forms of diffusive energy transport exist. In particular, work has been done on “neutrino bubble instabilities” in proto-neutron stars (Socrates et al. 2005) and “Coulomb bubble instabilities” in systems with anisotropic thermal conduction due to the presence of a magnetic field (Socrates, Parrish & Stone 2008).

All of this work on photon bubble and related instabilities has assumed a uniform background magnetic field, but gradients in the magnetic field can also drive instabilities. In particular, a medium may be vulnerable to magnetic interchange and undulatory Parker instabilities (Tserkovnikov 1960; Newcomb 1961; Parker 1966, 1967) if magnetic pressure gradients contribute significant support against gravity. Vertically stratified shearing box simulations indicate that such instabilities, not photon bubbles, appear to dominate the large scale dynamics of the surface layers of accretion disks (Blaes et al. 2007), though it is conceivable that photon bubbles would be relevant on smaller length scales that are unresolved in the existing simulations.

If both the equilibrium density and magnetic pressure decrease outward, then both the Parker and photon bubble unstable modes reduce to slow magnetosonic modes in the short wavelength limit. It is therefore likely that these two instabilities have nontrivial couplings in equilibria with both magnetic and radiation pressure gradients, and it is important to study this coupling in order to understand under what regimes and length scales each instability is likely to operate. This is the purpose of the present paper: we investigate local radiation MHD instabilities in equilibria that are supported against gravity by both radiation and magnetic pressure gradients.

We begin in section 2 by stating the basic radiation MHD equations and assumptions that we employ in our analysis. The perturbation equations are very complicated to analyze when we include both radiation and magnetic field physics, and much of the rest of the paper is devoted to various levels of approximation. The situation is simplest when one neglects gas pressure completely, as in Gammie’s (1998) original analysis of the photon bubble instability. We employ that approach in section 3, and find a single unstable mode at all wavelengths. There is a characteristic transition wavelength λ_{tran} above which the mode is Parker-like and below which the mode becomes the standard photon bubble instability, although the actual transition wavelength depends on the orientation of the wave vector of the perturbations. In section 4, we discuss the effects of finite gas pressure. Because much of the recent interest in photon bubble instabilities lies in accretion disks, we include the effects of differential rotation in section 5 and then discuss applications of our results to accretion disks in section 6. We finish by summarizing our findings in section 7. In the appendices we briefly show that our perturbation equations recover the basic properties of magnetic buoyancy instabilities derived by previous authors and show that, in contrast to the case of adiabatic perturbations (Newcomb 1961), the most rapidly growing Parker modes do not require large horizontal shear between field lines when radiation diffusion is rapid. We also present a more detailed derivation of our instability analysis with differential rotation.

2. EQUATIONS

Blaes & Socrates (2003) derived simplified versions of the general radiation MHD equations of Stone, Mihalas & Norman (1992), and we continue to use the same equations here, but with some additional assumptions. We assume that the gas and radiation temperatures are locked together and that the flux mean opacity κ is a constant (as would be true for Thomson scattering). The gravitational field $\mathbf{g} = -g\hat{\mathbf{z}}$, with $g > 0$ possibly being a function of height z , but independent of time as we neglect the effects of self-gravity. The equations then become

$$\frac{\partial \rho}{\partial t} + \nabla \cdot (\rho \mathbf{v}) = 0, \quad (1)$$

$$\rho \left(\frac{\partial \mathbf{v}}{\partial t} + \mathbf{v} \cdot \nabla \mathbf{v} \right) = -\nabla p + \rho \mathbf{g} + \frac{1}{4\pi} \mathbf{B} \cdot \nabla \mathbf{B} - \frac{1}{8\pi} \nabla B^2 + \frac{\kappa \rho}{c} \mathbf{F}, \quad (2)$$

$$\frac{\partial}{\partial t} (e + E) + \mathbf{v} \cdot \nabla (e + E) + \left(\frac{4}{3} E + \gamma e \right) \nabla \cdot \mathbf{v} = -\nabla \cdot \mathbf{F}, \quad (3)$$

$$\mathbf{F} = -\frac{c}{3\kappa\rho} \nabla E, \quad (4)$$

$$\frac{\partial \mathbf{B}}{\partial t} = \nabla \times (\mathbf{v} \times \mathbf{B}), \quad (5)$$

and

$$e = \frac{p}{\gamma - 1}, \quad p = \frac{\rho k_B T}{\mu}, \quad \text{and} \quad E = aT^4. \quad (6)$$

Here ρ is the fluid mass density, \mathbf{v} is the fluid velocity, p is the gas pressure, e is the gas internal energy density, T is the temperature, E is the radiation energy density, \mathbf{F} is the radiation flux, and \mathbf{B} is the magnetic field. Other symbols have their usual meanings: c is the speed of light, a is the radiation density constant, k_B is Boltzmann's constant, μ is the mean particle mass in the gas, and γ is the ratio of specific heats in the gas.

2.1. Equilibrium

We assume a static, vertically stratified, horizontally homogeneous equilibrium with purely horizontal magnetic field $\mathbf{B} = B(z)\hat{\mathbf{y}}$. The equilibrium radiation flux is $\mathbf{F} = F\hat{\mathbf{z}}$. The only differential equations that the equilibrium must satisfy are those of hydrostatic equilibrium,

$$\frac{d}{dz} \left(p + \frac{E}{3} + \frac{B^2}{8\pi} \right) = -\rho g, \quad (7)$$

radiative equilibrium,

$$\frac{dF}{dz} = 0, \quad (8)$$

and radiative diffusion

$$F = -\frac{c}{3\kappa\rho} \frac{dE}{dz}. \quad (9)$$

2.2. Perturbations

We linearize equations (1)-(6) about the general equilibrium, assuming a (t, x, y) -dependence of $\exp[i(k_x x + k_y y - \omega t)]$. We do not make any assumptions about the z -dependence of the perturbations as our background is a function of z and we in particular wish to include the effects of the background magnetic gradient to the maximum possible extent. Eliminating magnetic and radiation flux perturbations, we obtain five coupled ordinary differential equations:

$$-i\omega\tilde{\delta\rho} + ik_x\delta v_x + ik_y\delta v_y + \frac{d\delta v_z}{dz} - \frac{\delta v_z}{H_\rho} = 0, \quad (10)$$

$$i(\omega^2 - k_x^2 v_A^2 - k_y^2 v_A^2)\delta v_x - i\frac{k_x\omega}{\rho}\delta P - k_x v_A^2 \frac{d\delta v_z}{dz} + \frac{k_x v_A^2}{2H_{\text{mag}}}\delta v_z = 0, \quad (11)$$

$$i\omega^2\delta v_y - i\frac{k_y\omega}{\rho}\delta P + \frac{k_y v_A^2}{2H_{\text{mag}}}\delta v_z = 0, \quad (12)$$

$$\begin{aligned} & i v_A^2 \frac{d^2 \delta v_z}{dz^2} - \frac{3i v_A^2}{2H_{\text{mag}}} \frac{d\delta v_z}{dz} + i \left[\omega^2 - k_y^2 v_A^2 + \frac{v_A^2}{(H'_{\text{mag}})^2} \right] \delta v_z - k_x v_A^2 \frac{d\delta v_x}{dz} + \frac{k_x v_A^2}{H_{\text{mag}}} \delta v_x \\ & - \frac{\omega}{\rho} \frac{d\delta P}{dz} - \omega g \tilde{\delta\rho} = 0, \end{aligned} \quad (13)$$

and

$$\begin{aligned} & \frac{4cE}{3\kappa\rho} \frac{d^2 \tilde{\delta T}}{dz^2} - \left(8F - \frac{4cE}{3\kappa\rho H_\rho} \right) \frac{d\tilde{\delta T}}{dz} + \left[\frac{i\omega}{\Gamma_3 - 1} \left(p + \frac{4E}{3} \right) - \frac{4cE}{3\kappa\rho} (k_x^2 + k_y^2) \right] \tilde{\delta T} \\ & + F \frac{d\tilde{\delta\rho}}{dz} + \frac{i\omega\rho}{\Gamma_3 - 1} (c_i^2 - c_t^2) \tilde{\delta\rho} - \frac{\rho c_t^2 N^2}{g(\Gamma_3 - 1)} \delta v_z = 0. \end{aligned} \quad (14)$$

Here $v_A = B/\sqrt{4\pi\rho}$ is the Alfvén speed, $\tilde{\delta\rho} \equiv \delta\rho/\rho$, $\tilde{\delta T} \equiv \delta T/T$, and δP is the total thermal pressure perturbation,

$$\delta P \equiv \delta p + \frac{\delta E}{3} = \rho c_i^2 \tilde{\delta\rho} + \left(p + \frac{4E}{3} \right) \tilde{\delta T}. \quad (15)$$

The quantities $H_\rho(z)$, $H_{\text{mag}}(z)$, and $H'_{\text{mag}}(z)$ are measures of the local density and magnetic pressure scale heights,

$$H_\rho \equiv - \left(\frac{d \ln \rho}{dz} \right)^{-1} \quad H_{\text{mag}} \equiv - \left(\frac{d \ln B^2}{dz} \right)^{-1} \quad H'_{\text{mag}} \equiv \left[\frac{1}{2} \frac{d^2 \ln B^2}{dz^2} + \frac{1}{2} \left(\frac{d \ln B^2}{dz} \right)^2 \right]^{-1/2}. \quad (16)$$

We implicitly assume that H_ρ and H_{mag} are non-negative, i.e. that density and magnetic field do not increase outward. This is the regime of most relevance for the outer layers of stellar envelopes and the uppermost layers of accretion disks. The quantity N^2 is the square of the local Brunt-Väisälä frequency in the gas-radiation mixture,

$$N^2 = g \left[\frac{1}{\Gamma_1} \frac{d}{dz} \ln \left(p + \frac{E}{3} \right) - \frac{d \ln \rho}{dz} \right], \quad (17)$$

$c_i = (p/\rho)^{1/2}$ is the isothermal sound speed in the gas, $c_t = [\Gamma_1(p + E/3)/\rho]^{1/2}$ is the total adiabatic sound speed in the gas plus radiation mixture, and Γ_1 and Γ_3 are generalized adiabatic exponents (Chandrasekhar 1967),

$$\Gamma_1 = \frac{16E^2 + 60(\gamma - 1)Ee + 9\gamma(\gamma - 1)e^2}{9(e + 4E)(p + E/3)} \quad \text{and} \quad \Gamma_3 = \frac{16E + 3\gamma e}{3(e + 4E)}. \quad (18)$$

3. THE ZERO GAS PRESSURE LIMIT

The perturbation equations presented above are complicated and cannot be readily combined into a single ordinary differential equation. To make progress, we first consider short wavelengths where radiative diffusion is rapid, and follow Gammie (1998) by adopting the limit of zero gas pressure. After all, we are particularly interested in environments where magnetic and radiation pressures dominate greatly over gas pressure. The mathematical advantage of this approximation is that there is then no slow magnetosonic wave limit and the photon bubble instability appears at lowest order in the short wavelength limit. (For nonzero gas pressure, this analysis would only be valid for photon bubble wavelengths longer than a finite turnover wavelength; see section 4 below.) At the same time, the minimum unstable wavelength for the Parker instability also vanishes in the rapid diffusion limit if the gas pressure is zero. Hence the zero gas pressure limit enables us to explore the coupled photon bubble and Parker problem in the short wavelength WKB limit at lowest order. We shall find that the shortest wavelengths are always in the photon bubble regime, but if magnetic support dominates radiation support in the equilibrium, then there is a WKB transition wavelength longward of which the Parker instability becomes manifest.

Proceeding with a WKB ansatz that the z -dependence of all perturbations is $\exp(ik_z z)$, we obtain a seventh order dispersion relation. Taking the infinitely high wavenumber limit with $\omega \sim k^2$ gives the usual damped diffusion mode,

$$\omega = -i \frac{ck^2}{3\kappa\rho}, \quad (19)$$

where $k^2 \equiv k_x^2 + k_y^2 + k_z^2$. Doing the same thing with $\omega \sim k$ gives the two fast magnetosonic modes,

$$\omega^2 = k^2 v_A^2, \quad (20)$$

and the two Alfvén modes,

$$\omega^2 = k_y^2 v_A^2. \quad (21)$$

The remaining two modes describe the coupled Parker and photon bubble instabilities. Assuming that ω grows no faster than $k^{1/2}$ as $k \rightarrow \infty$, the lowest order terms in the dispersion relation become

$$\omega^2 k^4 + i\omega \left(\frac{4\kappa E}{3c} \right) k_y^2 k^2 + \left[\frac{k^2(k_x^2 + k_y^2)v_A^2}{4H_{\text{mag}}^2} + (k^2 k_x^2 + k^2 k_y^2 + 2k_z^2 k_y^2) \frac{\kappa F}{2H_{\text{mag}} c} - ik_z k_y^2 k^2 \frac{\kappa F}{c} \right] = 0. \quad (22)$$

Clearly as $k \rightarrow \infty$, the lowest order solution is given by

$$\omega^2 = i \frac{k_y^2 k_z}{k^2} \frac{\kappa F}{c}, \quad (23)$$

identical to the photon bubble dispersion relation in this regime (Gammie 1998).

On the other hand, if magnetic pressure gradients dominate radiation pressure gradients in supporting the medium against gravity, the last term in equation (22) can be small except at extremely short wavelengths. Neglecting this term, and also the linear term in ω for the moment, the dispersion relation gives for large magnetic pressure gradients

$$\omega^2 = -\frac{(k_x^2 + k_y^2)v_A^2}{4k^2 H_{\text{mag}}^2} \simeq -\frac{(k_x^2 + k_y^2)g}{2k^2 H_{\text{mag}}}, \quad (24)$$

which is the short wavelength Parker instability growth rate in this regime. This result agrees with the $c_i = 0$ and $k \rightarrow \infty$ (with $\omega \sim k^0$) limit of the Parker dispersion relation derived by Blaes et al. (2007) in their appendix. Their result assumed an isothermal medium, implying $F = 0$. However, we show in Appendix A that it is also valid for more general equilibria in which radiation and magnetic pressures dominate gas pressure, and radiative diffusion is rapid. [See equation (A15).]

Note that the pure Parker instability is a genuine exponentially growing instability in all space, whereas the pure photon bubble instability is an overstability of traveling waves. Nevertheless, the different wavenumber dependencies

of equations (23) and (24) indicate that a transition between photon bubble and Parker behavior will occur at a characteristic vertical wavenumber k_{tran} given by

$$k_{\text{tran}} \equiv \frac{2\pi}{\lambda_{\text{tran}}} \equiv \frac{v_A^2 c}{4H_{\text{mag}}^2 \kappa F}, \quad (25)$$

provided at least that k_x is not too large compared to k_y . Note that the photon bubble growth rate always declines with increasing k_x at fixed k . The photon bubble instability grows fastest when the perturbation gradients lie entirely in the plane defined by gravity and the magnetic field. The Parker growth rate is relatively unaffected by k_x in this zero gas pressure regime.

The corresponding transition wavelength can also be written in a more physically transparent fashion as

$$\lambda_{\text{tran}} = 4\pi H_{\text{mag}} \left(\frac{dP_{\text{rad}}/dz}{dP_{\text{mag}}/dz} \right), \quad (26)$$

where $P_{\text{rad}} = E/3$ is the radiation pressure and $P_{\text{mag}} = B^2/(8\pi)$ is the magnetic pressure. As magnetic pressure gradient forces become stronger compared to radiation pressure forces, λ_{tran} decreases, extending the long-wavelength range of the Parker instability at the expense of the short-wavelength range of the photon bubble instability.

For WKB to make sense with $k < k_{\text{tran}}$, we require $k_{\text{tran}} H_{\text{mag}} \gg 1$. This implies that magnetic support must dominate radiation pressure support in the equilibrium. If this is not true, then there is no WKB-accessible range of wavelengths where the Parker instability will be present (except for very short radial wavelengths: $k_x^2/k_y^2 \gg (k_{\text{tran}} H_{\text{mag}})^{-1}$). Assuming $k_{\text{tran}} H_{\text{mag}} \gg 1$, the middle term in the square brackets in equation (22) is negligible, leaving us with

$$\omega^2 + i \frac{k_y^2}{k^2} \frac{4E\kappa}{3c} \omega + \frac{(k_x^2 + k_y^2)v_A^2}{4H_{\text{mag}}^2 k^2} - i \frac{k_y k_z}{k^2} \frac{\kappa F}{c} = 0. \quad (27)$$

If damping (the linear term in ω) is negligible, the solution to this dispersion relation is

$$\omega = \pm \frac{k_y v_A}{2^{3/2} k H_{\text{mag}}} \left\{ \left[\left(\left(1 + k_x^2/k_y^2 \right)^2 + \frac{k_z^2}{k_{\text{tran}}^2} \right)^{1/2} - \left(1 + k_x^2/k_y^2 \right) \right]^{1/2} + i \left[\left(\left(1 + k_x^2/k_y^2 \right)^2 + \frac{k_z^2}{k_{\text{tran}}^2} \right)^{1/2} + \left(1 + k_x^2/k_y^2 \right) \right]^{1/2} \right\}. \quad (28)$$

The positive root is unstable: photon bubbles are recovered for $k_z \gg (1 + k_x^2/k_y^2)k_{\text{tran}}$, and Parker is recovered for $k_z \ll (1 + k_x^2/k_y^2)k_{\text{tran}}$.

To understand the role of the damping term, it is helpful to introduce the dimensionless quantity

$$b \equiv \frac{4E\kappa H_{\text{mag}}}{3c v_A} = 3 \left(\frac{c_r}{c} \right) \left(\frac{c_r}{v_A} \right) \kappa \rho H_{\text{mag}}, \quad (29)$$

where $c_r = (4E/9\rho)^{1/2}$ is the effective radiation sound speed. It is also convenient to scale the angular frequency of the mode with v_A/H_{mag} ,

$$\tilde{\omega} \equiv \frac{\omega H_{\text{mag}}}{v_A}. \quad (30)$$

Then the solution of the dispersion relation (27) may be written as

$$\tilde{\omega} = -i \frac{k_y^2 b}{2k^2} \pm \frac{k_y}{2k} \left[- \left(1 + \frac{k_x^2}{k_y^2} + \frac{k_y^2 b^2}{k^2} \right) + i \frac{k_z}{k_{\text{tran}}} \right]^{1/2} \quad (31)$$

or

$$\tilde{\omega} = -i \frac{k_y^2 b}{2k^2} \pm \frac{k_y}{2^{3/2} k} \times \left\{ \left[\left(\left(1 + k_x^2/k_y^2 + k_y^2 b^2/k^2 \right)^2 + \frac{k_z^2}{k_{\text{tran}}^2} \right)^{1/2} - \left(1 + k_x^2/k_y^2 + k_y^2 b^2/k^2 \right) \right]^{1/2} + i \left[\left(\left(1 + k_x^2/k_y^2 + k_y^2 b^2/k^2 \right)^2 + \frac{k_z^2}{k_{\text{tran}}^2} \right)^{1/2} + \left(1 + k_x^2/k_y^2 + k_y^2 b^2/k^2 \right) \right]^{1/2} \right\}. \quad (32)$$

Note that the mode with the upper (plus) sign is always unstable, in that the imaginary part of the frequency is always positive. The other root is always damped. The unstable mode again transitions smoothly from Parker for

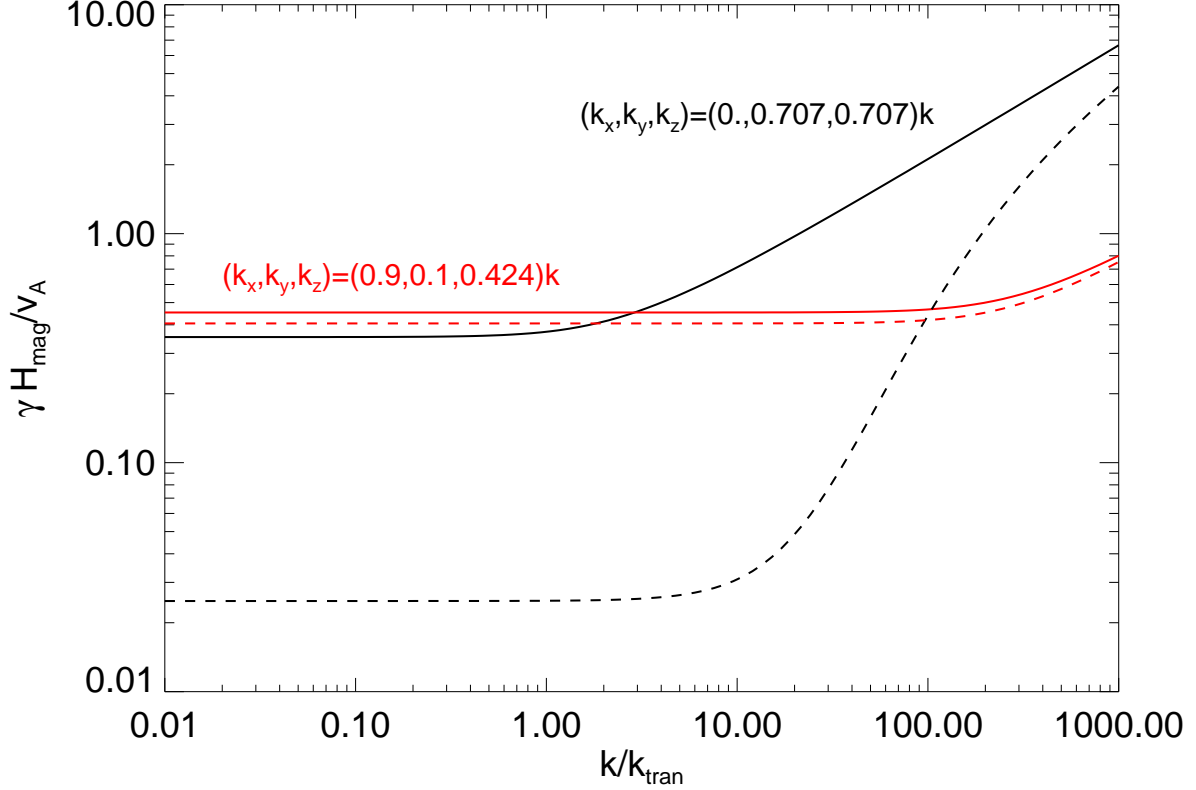


FIG. 1.— Scaled unstable mode growth rate $\gamma \equiv \text{Im}(\omega)$ as a function of the dimensionless wavenumber k/k_{tran} . The different colors are for different wavenumber orientations: $\hat{\mathbf{k}} = (0, 0.707, 0.707)$ (black) and $\hat{\mathbf{k}} = (0.9, 0.1, 0.424)$ (red). Solid curves have no damping ($b = 0$), while dashed curves have $b = 10$.

$k_z \ll (1 + k_x^2/k_y^2 + k_y^2 b^2/k^2)k_{\text{tran}}$ to photon bubble for $k_z \gg (1 + k_x^2/k_y^2 + k_y^2 b^2/k^2)k_{\text{tran}}$. The instability always becomes Parker-like for wave vectors in the $x - z$ plane, i.e. $k_y \rightarrow 0$.

Damping affects the Parker regime most. For $k_z \ll (1 + k_x^2/k_y^2 + k_y^2 b^2/k^2)k_{\text{tran}}$, we have

$$\tilde{\omega} \simeq -i \frac{k_y^2 b}{2k^2} \pm i \frac{k_y}{2k} \left(1 + \frac{k_x^2}{k_y^2} + \frac{k_y^2 b^2}{k^2} \right)^{1/2}. \quad (33)$$

Unless $k_y \rightarrow 0$, the growth rate of the unstable root is greatly reduced when damping is large ($b \gg 1$): $\tilde{\omega} \simeq i(1 + k_x^2/k_y^2)/(4b)$. On the other hand, photon bubbles are relatively unaffected by damping provided $k_z/k_{\text{tran}} \gg b^2$. If instead $b^2 \gg k_z/k_{\text{tran}} \gg 1$, then the real and imaginary parts of the unstable photon bubble frequency are markedly reduced:

$$\omega \simeq \frac{4E\kappa}{3c} \left(\frac{k_z}{4k_{\text{tran}}b^2} + i \frac{k_z^2 k^2}{16k_{\text{tran}}^2 k_y^2 b^4} \right). \quad (34)$$

Figure 1 illustrates these behaviors. The black curves show cases with $k_x = 0$ and zero damping ($b = 0$, solid curve) and finite damping ($b = 10$, dashed). Here the mode transitions from constant (Parker) growth rate at low wavenumbers to a (photon bubble) growth rate that increases as $k^{1/2}$ for high wavenumbers. The transition occurs at $k \sim k_{\text{tran}}$ with zero damping, and for k somewhere between 10 and 100 k_{tran} for $b = 10$. The latter is consistent with the transition wavenumber being given by $k_z \sim k_y^2 b^2 k_{\text{tran}}/k^2$, implying $k \sim (k_y/k)b^2 k_{\text{tran}} = 70.7k_{\text{tran}}$. For this wavenumber orientation, damping affects the Parker instability severely. The photon bubble growth rate is much less affected, however: little damping occurs for $k_z > b^2 k_{\text{tran}}$ or $k > (k/k_z)b^2 k_{\text{tran}} = 140k_{\text{tran}}$. The red pair of curves have the same damping parameters but now have wavenumbers oriented mostly in the $x - z$ plane. The transition to photon bubble behavior now occurs above a much higher wavenumber $k \sim (k_x^2/k_y^2)(k/k_z)k_{\text{tran}} \sim 200k_{\text{tran}}$. The Parker instability is insensitive to damping for this wavenumber orientation.

4. FINITE GAS PRESSURE EFFECTS

We now consider the effects of nonzero gas pressure on the coupled photon bubble/Parker instability. Finite gas pressure stabilizes the Parker instability at infinitely short wavelengths. Then radiative diffusion is so fast that $\delta T \approx 0$,

and instability only occurs for wavenumbers satisfying

$$|k_y| < \frac{(k_x^2 + k_y^2)^{1/2}}{k} k_P, \quad (35)$$

where

$$k_P \equiv \left(\frac{g}{2H_{\text{mag}} c_1^2} \right)^{1/2}. \quad (36)$$

[See equation (A12) in the Appendix.] If the magnetic pressure gradient is the dominant force in supporting the medium against gravity, then k_P reduces to $\approx g/(c_1 v_A) = v_A/(2H_{\text{mag}} c_1)$. In this case equation (35) can be written as $k_y v_A < g/c_1$ (ignoring wavenumber factors), which reveals its physical origin. Buoyancy is fundamentally what drives the Parker instability. Stability therefore requires that the magnetic tension not have time to restore the perturbed fluid elements on a buoyant rise time in the gas in the ambient gravitational field (which is largely determined by magnetic pressure gradients). Note, however, that the growth rate of the fastest mode of the instability is $\sim v_A/H_{\text{mag}}$, and occurs at a wavenumber much smaller than the marginally stable wavenumber k_P [equation (A16) in the Appendix].

In a medium that is only supported against gravity by gas and radiation pressure (no magnetic field gradients), finite sound speed affects the photon bubble instability by causing the growth rate to reach a fixed value once the wavenumber is high enough for the mode to become a slow magnetosonic mode. Provided that gas and radiation temperatures are thermally locked (as we are assuming throughout this paper), this turnover wavenumber is given by

$$k_T = \frac{\kappa F}{c c_1^2} \left(1 + \frac{3p}{4E} \right). \quad (37)$$

For wavenumbers greater than k_T , the instability growth rate asymptotes to a constant value $\sim k_T c_1$ when the magnetic pressure is much larger than the gas pressure p (Blaes & Socrates 2003).

Previous studies of the short wavelength photon bubble instability assumed a uniform equilibrium magnetic field, which therefore provides no support against gravity (Gammie 1998; Blaes & Socrates 2001, 2003). In this case, the turnover wavenumber k_T is approximately g/c_1^2 , i.e. the reciprocal of the gas pressure scale height (Blaes & Socrates 2003). When magnetic pressure gradients support the equilibrium, g/c_1^2 can be significantly larger than the true turnover wavenumber, implying that the asymptotic short wavelengths of the photon bubble instability (which have the highest growth rates) can be more easily resolved in numerical simulations than one might have expected from just the gas pressure scale height. On the other hand, the asymptotic growth rate can also be significantly smaller than the radiation pressure supported equilibrium estimate g/c_1 when magnetic gradients support the equilibrium.

We can write the three wavenumber scales in the problem as

$$k_{\text{tran}} = \frac{H_{\text{rad}}}{3H_{\text{mag}}^2} \left(\frac{v_A}{c_r} \right)^2, \quad (38)$$

$$k_T = \left(1 + \frac{3c_r^2}{c_1^2} \right) \frac{1}{4H_{\text{rad}}} \quad (39)$$

and

$$k_P = \left\{ \frac{1}{2H_{\text{mag}}} \left[\left(1 + \frac{3c_r^2}{c_1^2} \right) \frac{1}{4H_{\text{rad}}} + \frac{v_A^2}{2c_1^2 H_{\text{mag}}} + \frac{1}{H_\rho} \right] \right\}^{1/2}, \quad (40)$$

where $H_{\text{rad}} \equiv -(d \ln E/dz)^{-1}$ is the radiation pressure scale height, k_T and k_P are the photon bubble turnover and Parker cutoff wavenumbers, respectively. We emphasize that these expressions are only valid in the limit of rapid radiative diffusion. To study our problem around these wavenumber regimes with WKB methods, we need $kH \gg 1$, where k is any of k_{tran} , k_T or k_P and H is any of the scale heights.

As we showed in section 3, our $c_1 = 0$ WKB dispersion relation (27) agrees with previously published photon bubble and Parker instability growth rates. This suggests that taking the z -dependence of all perturbations to be $\exp(ik_z z)$ without combining the perturbation equations first may prove useful even in the finite but small (compared to magnetic and radiation pressures) gas pressure regime. We solved the resulting dispersion relation numerically. Figure 2 shows results for an illustrative set of parameters. The photon bubble growth rate asymptotes to a finite value beyond the turnover wavenumber k_T because the gas pressure is no longer exactly zero.

In both Figures 1 and 2, note that there is no sign of photon bubbles for low wavenumber ($k \ll k_{\text{tran}}$) where diffusion will eventually be slow. In particular, our low wavenumber growth rate agrees with that of the Parker instability, but not with the Arons (1992) photon bubble result. Thus if magnetic gradients are large enough that k_{tran} corresponds to wavelengths in the rapid diffusion regime, then the slow diffusion version of the photon bubble instability may not exist. However, a non-WKB analysis is necessary to verify this conclusively.

It is also possible in principle for the maximum Parker growth rate to be higher than that of the photon bubble instability. Analytically, this occurs when the photon bubble growth rate obtained by Blaes & Socrates (2003) (their equation 93) exceeds the Parker growth rate stated in equation (A13). In the limit that the medium is magnetically supported, and the gas pressure is much smaller than radiation and magnetic pressures, this comparison means that

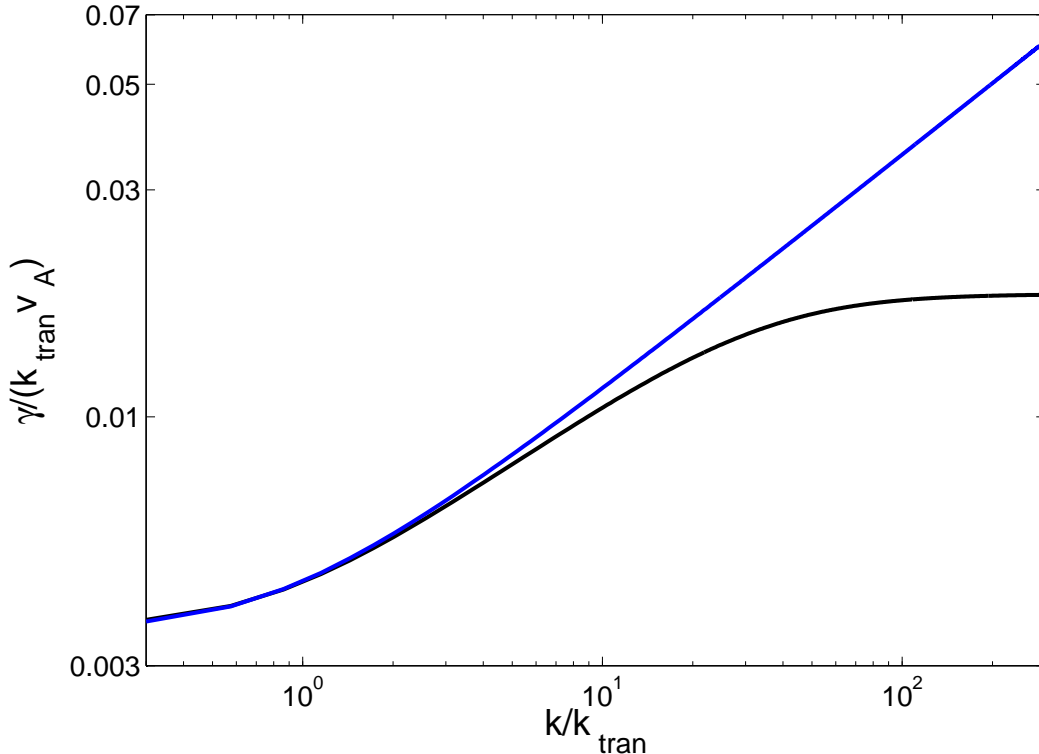


FIG. 2.— Instability growth rate $\gamma \equiv \text{Im}(\omega)$ (black curve) in units of $k_{\text{tran}}v_A$ versus total wavenumber in units of k_{tran} , for a wavenumber orientation $k_x : k_y : k_z = \sin(\pi/12) : 1 : 1$. Here we set all the scale heights in the calculation to be equal: $H_{\text{mag}} = H_\rho = H_{\text{rad}}$. The sound speeds, Alfvén speed, and damping parameter satisfy $c_i/v_A = 0.01$, $c_r/v_A = 0.1$, and $b = 0.01$. This implies $k_{\text{tran}}H \simeq 33$, $k_P/k_{\text{tran}} \simeq 50$, and $k_T/k_{\text{tran}} \simeq 75$. The blue curve in this figure shows the growth rate from the analytic zero gas sound speed expression (32).

Parker dominates if $v_A/H_{\text{mag}} \gg (c_r/H_{\text{rad}})(c_r/c_i)$. Provided the scale heights are comparable, this is equivalent to the condition that $k_P < k_{\text{tran}}$, so that the Parker growth rate cuts off and decreases down to the asymptotic photon bubble growth rate. In this case the Parker instability transitions into the photon bubble instability when k exceeds k_P , which is *less* than the transition wavenumber k_{tran} for zero gas pressure. For finite gas pressure, the Parker growth rate can exceed the photon bubble growth rate even without this ordering of the characteristic wavenumbers. We will later present a finite gas pressure example of this from a numerical simulation of accretion disk vertical structure in section 6 below.

5. EFFECTS OF ROTATION AND SHEAR

Motivated by the fact that both Parker and photon bubble instabilities are driven by vertical gradients, and by possible applications to stellar envelopes and atmospheres, our analysis so far has assumed a static equilibrium. However, there has been considerable recent interest in photon bubble physics in radiation dominated accretion disks. Such flows are differentially rotating, and before one can apply our results to such flows, one has to account for the effects of rotation and shear. Such effects were first examined by Shu (1974) for the Parker instability, and by Blaes & Socrates (2001) in the case of the photon bubble instability restricted to axisymmetric perturbations.

In the spirit of the short wavelength WKB approximation that we have been using, we restrict attention to a local, corotating patch of a differentially rotating disk and use the fluid equations describing a shearing box (Goldreich & Lynden-Bell 1965; Hawley, Gammie & Balbus 1995) with coordinate axes (x, y, z) aligned with the radial, azimuthal, and vertical directions, respectively. Appendix B presents a detailed analysis of the coupled Parker-photon bubble problem, again assuming negligible gas pressure as we did in section 3 above. Provided $k_{\text{tran}}H_{\text{mag}} \gg 1$, the azimuthal component ξ_y of the small amplitude Lagrangian displacement of perturbations satisfies the differential equation

$$\frac{\partial^2 \xi_y}{\partial t^2} + \frac{k_y^2}{k^2} \frac{4E\kappa}{3c} \frac{\partial \xi_y}{\partial t} - \frac{(k_x^2 + k_y^2)v_A^2}{4H_{\text{mag}}^2 k^2} \xi_y + i \frac{k_y^2 k_z}{k^2} \frac{\kappa F}{c} \xi_y = 0. \quad (41)$$

In the absence of differential rotation, all the coefficients of this equation would be independent of time. We could then assume a complex exponential time-dependence $\xi_y \propto \exp(-i\omega t)$ and recover the static equilibrium dispersion relation (27) that we derived above. As we discuss in more detail in Appendix B, Coriolis forces are negligible provided the WKB approximation is valid.

However, the shear due to the differential rotation of the equilibrium flow has a more important effect. This shear means that the radial wavenumber k_x depends on time: $k_x(t) = k_{x0} + q\Omega t k_y$, where k_{x0} is the initial value of k_x , q

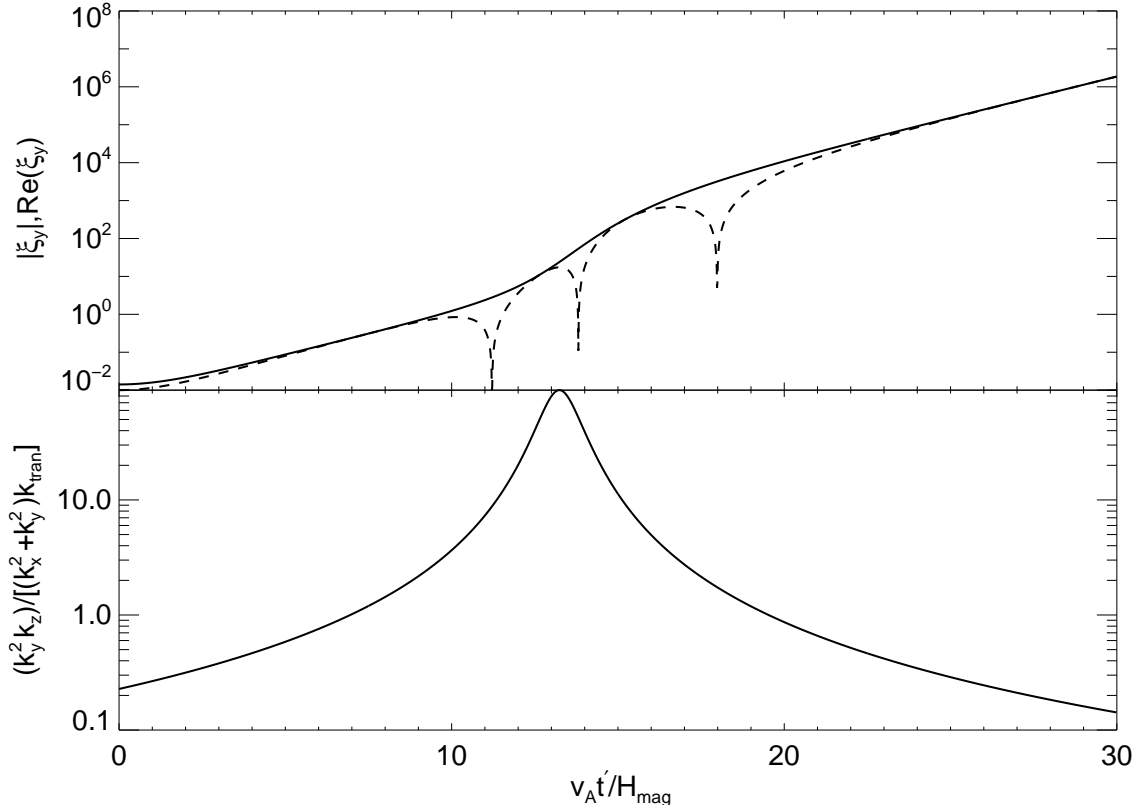


FIG. 3.— Upper plot: modulus (solid curve) and real part (dashed curve) of the azimuthal component of the Lagrangian displacement, in arbitrary units, as a function of time in a shearing box with negligible gas pressure. This particular case assumed dimensionless parameter values of $b = 0$ (i.e. negligible radiative damping), $\Omega H_{\text{mag}}/v_A = 1$, $q = 3/2$, $k_z/k_{\text{tran}} = 90$, and $(k_{x0}, k_y, k_z) = (-0.993, 0.05, 0.107)k$. Lower plot: the dimensionless ratio $k_y^2 k_z / (k_x^2 + k_y^2) k_{\text{tran}}$ as a function of time for the same parameters. The instability is in the Parker regime when this ratio is less than of order unity, and in the photon bubble regime otherwise.

is the shear parameter ($3/2$ for a Keplerian accretion disk), and Ω is the angular velocity of the local patch of disk. The exponential growth rates of the static equilibrium analysis will therefore only be valid so long as these growth rates are faster than the time it takes the radial wavenumber to change significantly in time. For a magnetically supported medium, this implies that $(k_{x0}^2/k^2)(k_{\perp}^2/k_y^2) \gg q^2$ for the Parker regime, and $(k_{x0}^2/k^2)(|k_z|/k_{\text{tran}}) \gg q^2$ for the photon bubble regime. The latter is easier to satisfy than the former, as the transition from Parker to photon bubble occurs when $|k_z|/k_{\text{tran}} > k_{\perp}^2/k_y^2$, assuming negligible damping. On the other hand, if radiation pressure supports the equilibrium, then shear will not affect the exponential growth of photon bubbles provided $(k_{x0}^2/k^2)|k_z|H_{\text{rad}} \gg q^2$, which is essentially equivalent to the WKB condition. Short wavelength photon bubbles are therefore generally less affected by shear than Parker modes.

Note that if these conditions are not satisfied and/or the instabilities fail to reach the nonlinear regime before the waves start to shear, then the character of the unstable driving can change with time. For example, a strongly leading nonaxisymmetric perturbation (e.g. $k_y > 0$ and k_{x0} large and negative) could start in the Parker regime, then flip to the photon bubble regime as the wave swings from leading to trailing ($k_x \sim 0$), and then flip back to the Parker regime as the perturbation becomes strongly trailing (k_x large and positive). We illustrate this linear regime behavior in Figure 3 which depicts a numerical solution to equation (41). Nonaxisymmetric photon bubbles inevitably enter the Parker regime unless they become nonlinear first as the wavevector shears to be strongly trailing. But again, photon bubbles whose vertical wavelengths are short enough should be able to grow much faster than the shear rate.

Axisymmetric ($k_y = 0$) perturbations are immune to these shear effects, but the photon bubble growth rate vanishes for such perturbations. Photon bubbles necessarily require wave vectors which are neither entirely perpendicular or along the equilibrium magnetic field (Blaes & Socrates 2003). Because we are considering equilibria with vertical magnetic gradients, we restricted consideration to equilibrium magnetic fields that are entirely in the azimuthal (y) direction. These are generally the dominant magnetic field components even in a turbulent accretion disk because of the differential rotation. But other components are present, especially in the surface layers if large-scale Parker modes are able to grow (Blaes et al. 2007). Axisymmetric photon bubbles on an equilibrium with magnetic field components in all directions have growth rates that are proportional to the square of the ratio of the non-azimuthal field components to the total magnetic field (Gammie 1998; Blaes & Socrates 2001, 2003), and hence have slower growth rates than nonaxisymmetric photon bubbles in a medium dominated by azimuthal fields.

Our discussion in this section has assumed negligible sound speed c_i in the gas alone. As we will see in the next section,

radiation MHD simulations of local patches of accretion disks generally produce conditions in which $k_T > k_P > k_{\text{tran}}$. Hence the main thing that finite gas sound speed introduces is a limit $\sim k_T c_i$ to the short wavelength photon bubble growth rate for $k \gtrsim k_T$. In that very short wavelength regime, photon bubbles continue to be immune to the shear rate. For a radiation pressure supported medium, this merely requires $\Omega H_{\text{rad}}/c_i \gg q$, which is clearly satisfied because $\Omega \sim c_r/H_{\text{rad}}$. For a magnetically supported medium, this requires instead that $c_r^2/(c_i v_A) \gg q$ provided the radiation pressure and magnetic pressure scale heights are comparable. This in turn is equivalent to the condition that $k_T \gg k_{\text{tran}}$, which we find to be generally true.

To summarize, in a medium supported by radiation pressure, rotation and shear do not significantly affect the photon bubble regime provided we are considering vertical wavelengths that are short enough for the WKB approximation to be valid ($|k_z|H \gg 1$). In a magnetically supported medium, photon bubbles grow quickly compared to the shear rate provided the vertical wavelength is much shorter than the transition wavelength λ_{tran} . Shear is more important near or longer than the transition wavelength; i.e. in the Parker regime, modes can be more affected by shear, unless they are associated with very short radial wavelengths.

6. APPLICATIONS TO ASTROPHYSICAL ACCRETION DISKS

In this section we investigate the relevance of photon bubble and Parker instabilities to the surface layers of high luminosity accretion disks, using recent stratified shearing box, radiation-MHD simulations as a guide to expected local conditions. In particular, we use data from simulations 0528a of Krolik et al. (2007) and Blaes et al. (2007), and 1112a and 0519b of Hirose et al. (2009). The simulations represent local patches of accretion disks at 30 (1112a and 0519b) and 150 (0528a) gravitational radii around a 6.62 solar mass black hole, and have time-averaged, volume-integrated radiation to gas pressure ratios of approximately 1 (0528a), 7 (1112a), and 70 (0519b). We time and horizontally average the fluid variables in each simulation in order to have an approximate vertically stratified equilibrium in which to explore the instabilities that we have calculated above. All time averages of the simulation data neglect the first ten orbits during which the magnetorotational instability was still developing.

Figure 4 depicts the time and horizontally-averaged vertical profiles of radiation, gas and magnetic pressures in each of the three simulations. (The height z on the horizontal axis in these and other figures in this paper is in units of the scale height H of the initial condition of the simulations: approximately 3.1×10^6 cm for 0528a, 1.46×10^6 cm for 1112a and 4.37×10^6 cm for 0519b. This initial scale height is comparable to the actual total pressure scale height of the resulting time-averaged structure.) In the outer layers of the accretion disk in all three simulations, magnetic pressure greatly dominates gas pressure, and also generally dominates radiation pressure. As a result, the Parker instability generally controls the dynamics of these layers on the scales resolved by the simulations (Blaes et al. 2007). However, Figure 4 shows that at the highest levels of radiation to gas pressure ratio, radiation pressure is becoming comparable to magnetic pressure in supporting the disk outer layers. We therefore expect the photon bubble instability to be more prominent in higher radiation pressure systems as the transition wavenumber k_{tran} decreases with decreasing magnetic to radiation pressure ratio, assuming comparable radiation and magnetic pressure scale heights. Photon bubbles, rather than Parker instability, may control the surface layer dynamics at high levels of radiation pressure support.

Beyond pressure considerations, the medium also needs to be optically thick (but not so thick as to impede radiative diffusion) at a particular wavelength in order to drive the photon bubble instability at that wavelength. This is because diffusive radiative transport is essential for producing radiative amplification when the opacity is dominated by Thomson scattering (Blaes & Socrates 2003). However, Figure 5 shows that the photon bubble turnover wavelength becomes optically thin to electron scattering beyond $|z/H|$ of approximately 2.1 and 2.7 for simulations 0519b and 1112a, respectively. This means that the instability cannot exist at wavenumbers higher than k_T and thus will not achieve its maximum growth rate near the disk photosphere. These simple estimates mean that only longer wavelength photon bubble modes can grow in the upper layers of such accretion disks. Nevertheless, these slower, longer wavelength modes might still develop into shock trains: approximate nonlinear solutions with finite optical depths have been explored by Begelman (2006b). The Parker instability, on the other hand, is not driven by radiative diffusion and hence is not subject to such optical depth restrictions.

Incidentally, Figure 5 also shows that $k_T > k_P > k_{\text{tran}}$ in all three simulations. With the exception of 0528a (see Figure 9) where the gas pressure in the disk upper layer is not negligibly small, the growth rate dependence on wavenumber therefore resembles that depicted in Figure 2. As shown in that figure, the Parker instability transitions into the photon bubble instability at short wavelengths before magnetic tension would introduce a cutoff. Note, however, that the photon bubble instability would never reach the asymptotic growth rate depicted in that figure because the turnover wavelength $2\pi/k_T$ is optically thin.

Figure 6 shows the same three characteristic wavelengths as a function of height in the simulations, now scaled by the azimuthal grid cell size. Also shown are the characteristic wavelengths that demarcate the rapid ($\lambda < \lambda_R$) and slow ($\lambda > \lambda_S$) radiative diffusion regimes for acoustic perturbations (Blaes et al. 2007):

$$\lambda_R \equiv \frac{2\pi c}{3c_i \kappa \rho} \left(\frac{4E}{e + 4E} \right) \left(\frac{c_i}{c_t} \right)^2 \quad (42)$$

and

$$\lambda_S \equiv \frac{c_t}{c_i} \lambda_R. \quad (43)$$

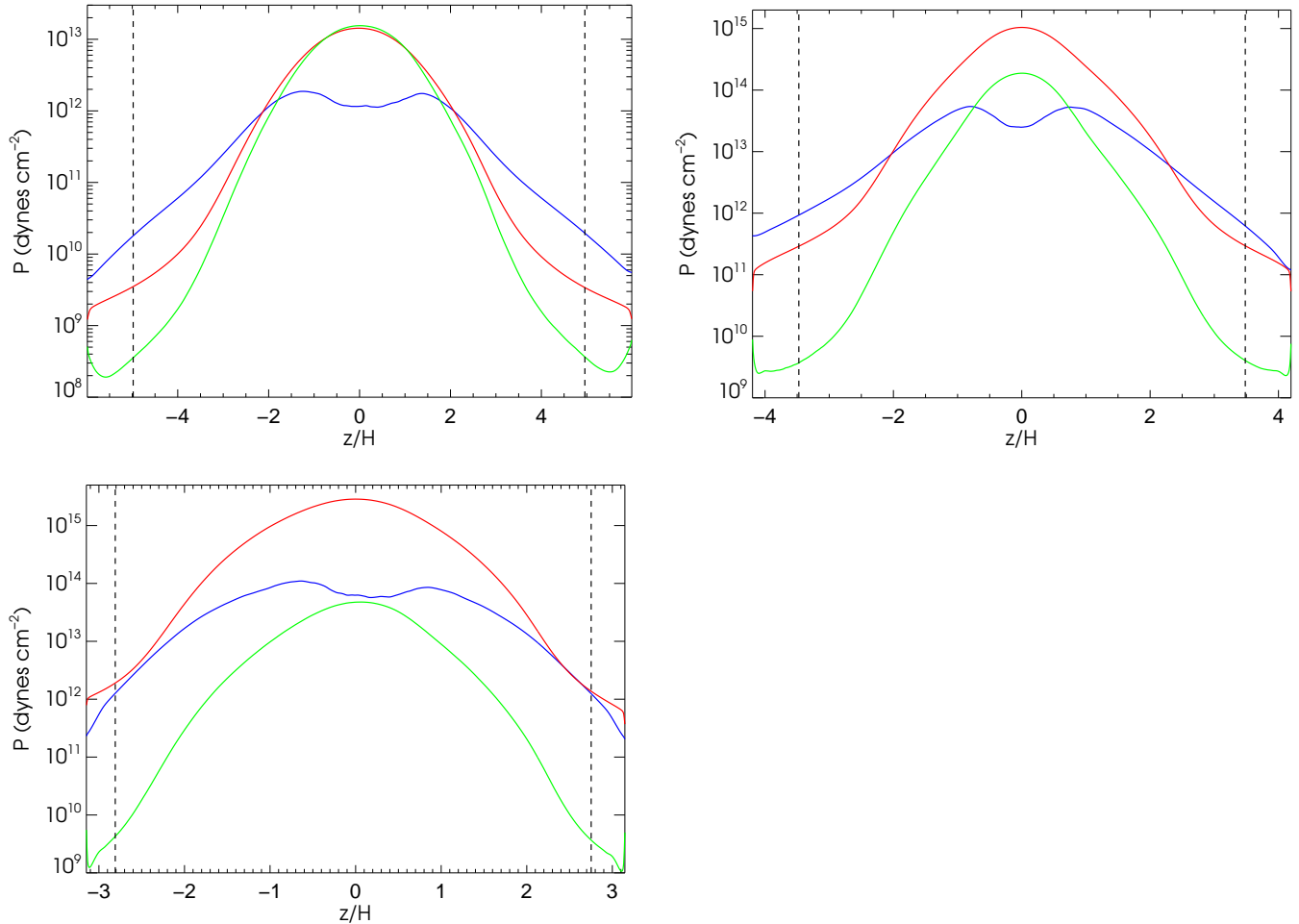


FIG. 4.— Horizontal and time averaged radiation (red), magnetic (blue) and gas (green) pressures as a function of height in local shearing box accretion disk simulations 0528a (top left), 1112a (top right) and 0519b (bottom). Vertical dashed lines indicate the locations of the Rosseland mean (mostly electron scattering) photospheres in the time-averaged structures. Note that the radiation to magnetic pressure ratio in the disk surface layers increases with increasing overall (volume integrated and time averaged) radiation to gas pressure ratio.

Most of the results of this paper only apply in the rapid diffusion regime ($\lambda < \lambda_R$, i.e. below the green curves in Figure 6). We therefore see that Parker instabilities with small k_x cannot exist in the rapid diffusion regime in the highest radiation to gas pressure ratio simulation 0519b, as they have already transitioned into photon bubbles. This reflects the fact that we noted above that magnetic pressure is not dominant over radiation pressure in the surface layers of this simulation. However, large k_x modes (i.e. those with large radial shear between the field lines) will still be Parker-like in character even in the rapid radiative diffusion regime, and the magnetic field and density structure in this simulation still shows evidence of Parker instability (Blaes et al. 2011).

Photon bubbles can reach their maximum growth rate in a narrow range of depths in simulations 0519b and 1112a, where radiative damping becomes small compared to the photon bubble asymptotic growth rate and the turnover wavelength is optically thick to scattering. Here the photon bubbles may evolve into nonlinear shock trains (Begelman 2001) that can propagate outward into the photosphere and potentially produce observable signatures. However, Figure 6 shows that the turnover wavelength in 1112a and 0519b is at most a few times larger than the grid zone size in the region where k_T is in the rapid diffusion limit, which means that the simulation cannot resolve the fastest growing photon bubble modes, even if they can physically exist in this region.

Figure 7 shows the asymptotic, short wavelength, photon bubble growth rate (black curve), as well as the rapid diffusion Parker growth rate (blue curve), in the radiation dominated simulations 1112a and 0519b. The plots are restricted to a range of heights where radiative damping of photon bubbles is small enough so that they are unstable, and where the turnover wavelength is optically thick. Within this range, we only show the Parker growth rates where the cutoff wavelength λ_P is in the rapid diffusion regime, where the analysis of this paper is valid. Photon bubbles grow faster than Parker in this range of heights, and so in principle could be important, but as we noted above, the simulations cannot resolve these fastest growing wavelengths. Note that the midplane regions, where most of the magnetorotational turbulence is acting, are not photon bubble unstable.

Figure 8 shows the same information for simulation 0528a, and may explain why Blaes et al. (2007) did not observe the photon bubble instability in this $P_{\text{rad}} \approx P_{\text{gas}}$ simulation. There the transition wavelength in the upper layers

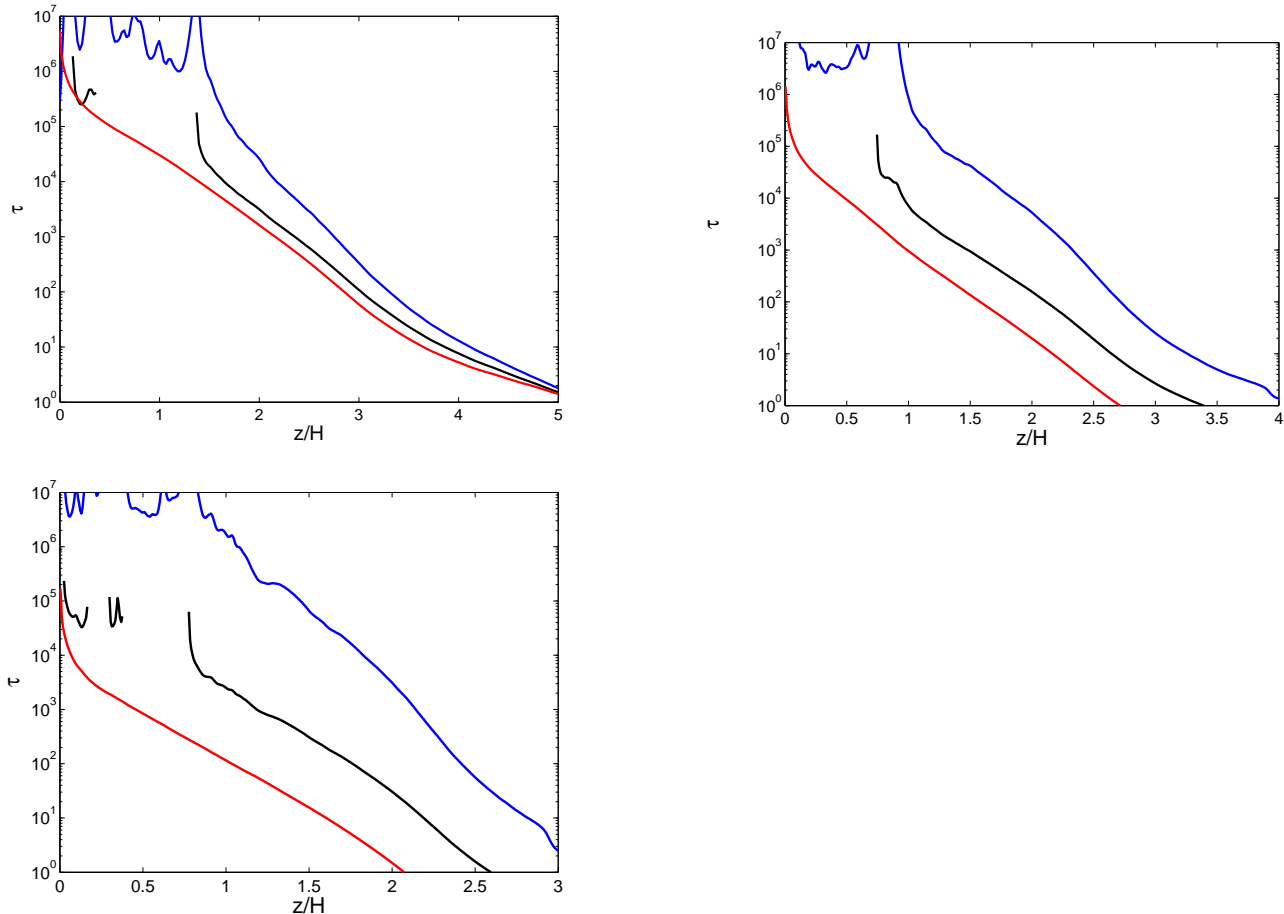


FIG. 5.— Optical depth of the characteristic wavelengths to electron scattering as a function of height for the horizontally and time-averaged structures in simulations 0528a (top left), 1112a (top right), and 0519b (bottom). Red, black and blue curves represent the photon bubble turnover wavelength, Parker cutoff wavelength and photon bubble/Parker transition wavelength, respectively.

is moderately optically thick to electron scattering, which suggests that photon bubbles can physically exist in the simulated disk. However, Figure 8 shows that Parker is the dominant instability, at least for $|z/H| \gtrsim 2.5$, where λ_P is in the rapid diffusion regime. Figure 9 shows the growth rate as a function of wavenumber at a representative height ($z/H = 3.5$) in the disk upper layer and further illustrates this conclusion. Closer to the midplane, radiative damping dominates over photon bubbles in the short wavelength limit. Note that our plotted results are comparable to and consistent with the growth rates estimated by Blaes et al. (2007) at two specific epochs in this simulation. Those authors did not know how Parker and photon bubbles couple together, but we have demonstrated here that the maximum growth rates of the individual instabilities are in fact unaltered.

7. CONCLUSIONS

We expanded previous studies of photon bubble instabilities to include background magnetic field gradients, thereby introducing a coupling between photon bubble and Parker instabilities. Our first main result was obtained assuming negligible gas pressure in the equilibrium, which in principle allows the photon bubble and Parker instabilities to exist out to very short wavelengths. There we identified a finite transition wavenumber k_{tran} between the photon bubble and Parker instabilities. The instability is Parker-like for $k < k_{\text{tran}}$ and photon bubble-like for $k > k_{\text{tran}}$, although strong horizontal shear between neighboring magnetic field lines (i.e. large k_x) pushes the Parker-like range to higher wavenumber.

We then proceeded to a naive WKB study including finite gas pressure. We numerically found approximately the same transition wavenumber. Moreover, finite gas pressure introduces finite photon bubble turnover and Parker cutoff wavenumbers (k_T and k_P , respectively). For $k_P < k_{\text{tran}}$, we see a sharp growth rate decrease above $k \simeq k_P$, while the photon bubble growth rate becomes constant in k for $k > k_T$. Once again, the growth rates of both instabilities agree with previous results in all wavenumber regimes. We also derived the scaling of the important wavenumbers k_T , k_P and k_{tran} as functions of background parameters in equations (38)-(40). Note that the results of this paper can only be applied to backgrounds where the characteristic wavenumbers k_{tran} , k_P and k_T satisfy the WKB condition $kH \gg 1$.

We also developed a WKB analysis of the coupled Parker/photon bubble problem including the effects of differential rotation. Photon bubbles are not significantly affected by shear and rotation provided their wavelengths are short enough. On the other hand, Parker modes can be affected by shear unless they have short radial wavelengths. This

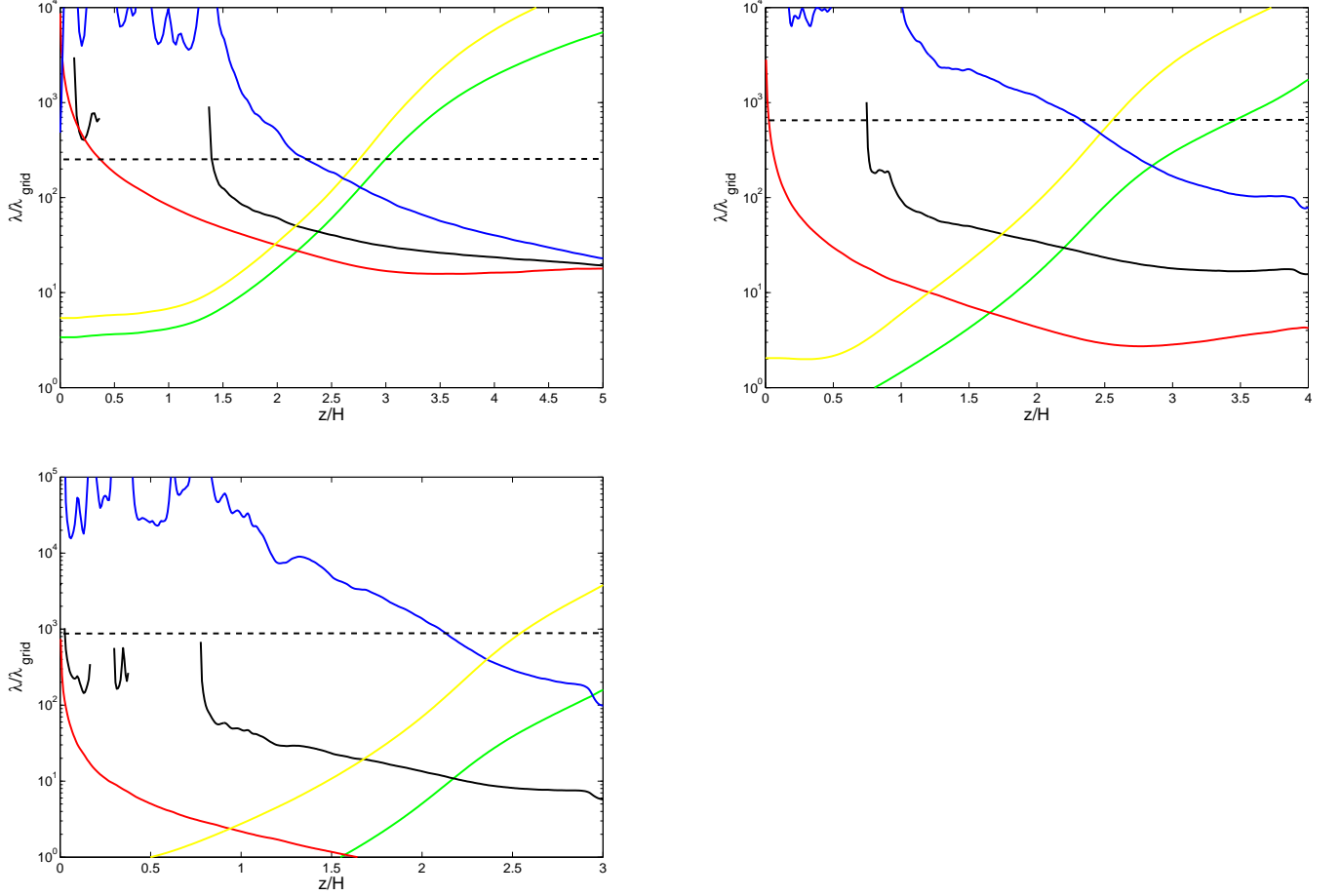


FIG. 6.— The critical wavelengths λ_{tran} (blue), λ_{P} (black) and λ_{T} (red), normalized by the azimuthal grid cell size, as a function of height for the horizontally and time-averaged structures of simulations 0528a (top left, $P_{\text{rad}} \cong P_{\text{gas}}$), 1112a (top right, $P_{\text{rad}} \cong 7P_{\text{gas}}$) and 0519b (bottom, $P_{\text{rad}} \cong 70P_{\text{gas}}$). The green curves indicate the wavelength λ_{R} below which radiative diffusion is rapid for acoustic perturbations, and the yellow curves indicate the wavelength λ_{S} above which radiative diffusion is slow for acoustic perturbations. The gaps in the black curves indicate regions where the horizontal and time averaged magnetic pressure increases vertically outward. Our WKB analysis is only valid below the horizontal dashed lines, which indicate the value of $2\pi H$ in each of the simulations.

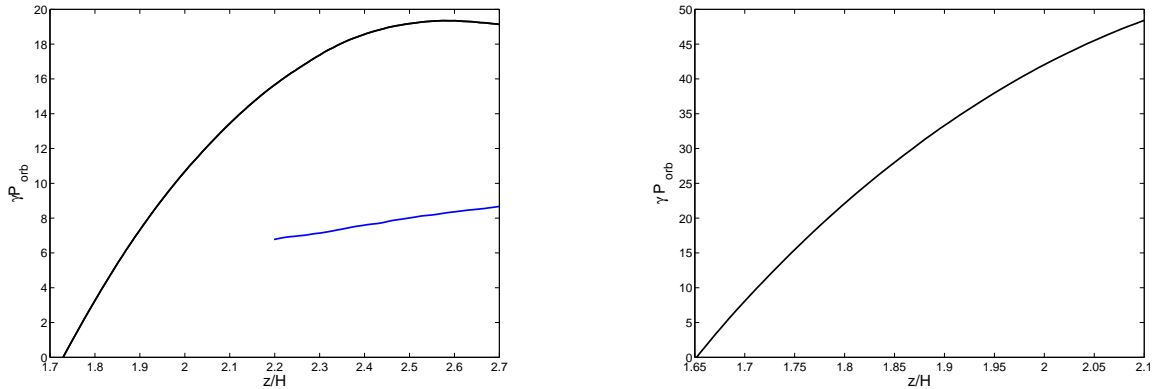


FIG. 7.— Maximum rapid diffusion Parker growth rate (blue) [from equation (A13)] and the asymptotic short-wavelength photon bubble growth rate [black, based on equation (93) of Blaes & Socrates (2003)] as a function of height from horizontal and time averaged data above the midplane in simulations 1112a (left) and 0519b (right). The plotted growth rates are scaled with the local orbital period for each simulation. The wave vector orientation is $\hat{\mathbf{k}} = (0, \cos(\pi/4), \sin(\pi/4))$. At heights below those shown in the plots, photon bubble growth is suppressed by radiative damping, while at heights above those shown, the photon bubble turnover wavelength is optically thin, so that the short wavelength asymptotic growth rates cannot be achieved. Note that the plotted Parker growth rate is only valid within regions where the cutoff wavelength k_{P} is in the rapid diffusion regime, which in the case of 0519b is above the plotted range.

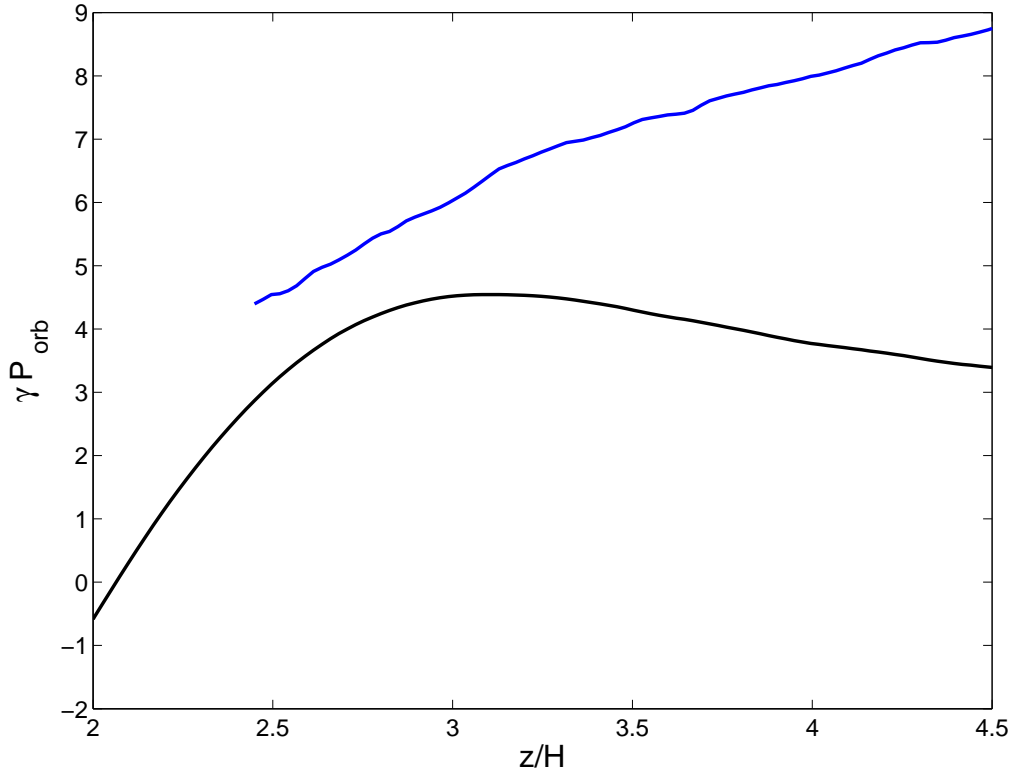


FIG. 8.— Same as Figure 7 but for simulation 0528a.

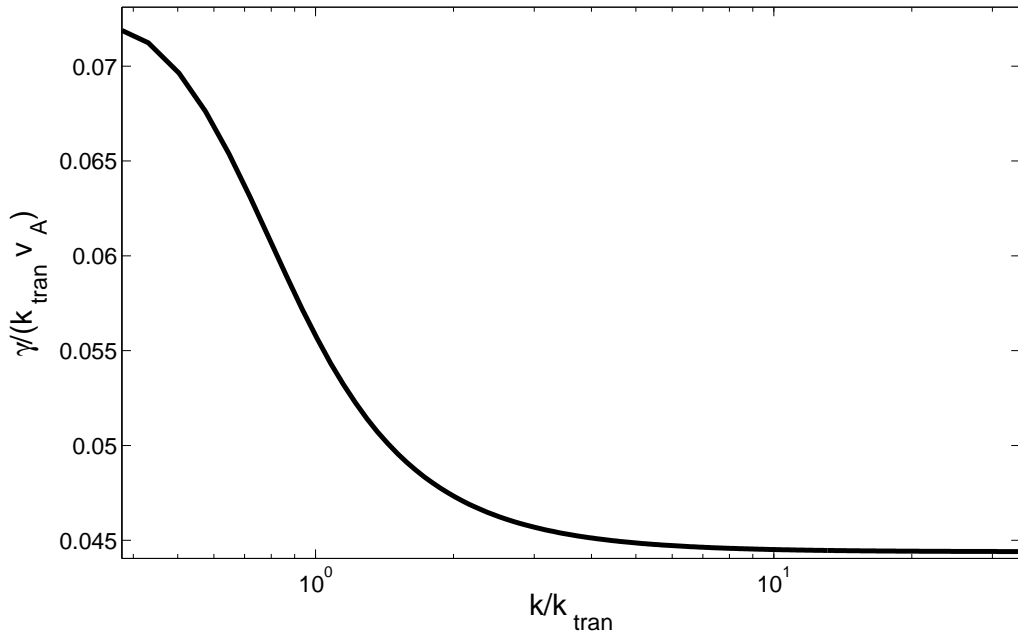


FIG. 9.— Instability growth rate as a function of wavenumber for parameters taken from the horizontal and time averaged simulation 0528a results at $z/H = 3.5$. We see that the maximum Parker instability growth rate is indeed higher than the photon bubble asymptotic growth rate in this case, in agreement with Figure 8.

is equivalent to the condition of strong horizontal shear between neighboring field lines that expands the Parker-like range to higher wavenumber.

We applied our results to analyze radiation MHD shearing box accretion disk simulations 0528a, 1112a and 0519b with volume integrated radiation to gas pressure ratios of 1, 7 and 70, respectively. We found that the asymptotically growing short wavelength photon bubble instability is not likely to exist in the upper layers of both 1112a and 0519b because the turnover wavelength becomes optically thin to electron scattering in the photosphere. For 0528a, the undulatory Parker instability in the rapid diffusion regime dominates over photon bubbles in the upper layers. On the other hand, radiative damping destroys the photon bubbles near the midplane in all three simulations, and photon bubbles may exist at the asymptotic growth rate only in a narrow range of heights. Even there it is not clear whether the turbulent conditions would allow the photon bubbles to grow unimpeded. Last but not least, the grid cell sizes of current radiation pressure dominated simulations are inadequate to fully resolve the turnover wavelength of the photon bubble instability, so that the fastest growing wavelengths cannot manifest themselves. Higher resolution radiation pressure dominated simulations may reveal this instability.

While accretion disk applications have been our focus, much of the analysis of this paper applies to static media, and magnetized stellar envelopes are clearly another area where this physics would be relevant. Generalizing the simulations by Turner et al. (2005) of magnetized, vertically stratified static equilibria to include magnetic pressure gradients would be interesting in order to explore how the photon bubble and Parker instabilities interact in the nonlinear regime. Even if short wavelength photon bubbles have faster linear growth rates than the longer wavelength Parker modes, Turner et al. (2005) have shown that the resulting nonlinear shock trains merge, causing the distances between adjacent shocks and the density contrast to grow until the magnetic field buckles (or until only one wavelength fills the simulation domain). This field line buckling may resemble the nonlinear development of the undulatory Parker instability, and it may be that both instabilities ultimately lead to a similar nonlinear outcome, at least in some regimes.

Finally, we stress an important caveat to our work: the photon bubble-Parker transition regime of our numerical finite gas pressure results do not readily apply when $c_i \geq v_A$, c_r or $c_t \geq v_A$, due to limitations of the WKB method discussed in section 4. Such regimes can exist in the portion of the accretion disk within and just outside the MRI unstable region, where the gravitational potential energy is dissipated into heat (Hirose et al. 2009). The behavior of the Parker-photon bubble transition in this region may be important for understanding how accretion power is transported outward. This is a difficult problem that may deserve further future work.

We owe a debt of gratitude to Ellen Zweibel for illuminating many aspects of the physics of the Parker instability. We also thank the referee for constructive criticism and for suggesting that we look more carefully at the issues of rotation and shear when considering accretion disk applications. We have benefited from helpful discussions with L. Bildsten, M. Block, K. Choiu, E. Gallo, J. Jacob, E. Rykoff, N. Turner, E. Newton and D. Harsono. This work was supported in part by NSF grants AST-0307657 and AST-0707624.

APPENDIX

MAGNETIC BUOYANCY INSTABILITIES IN THE ABSENCE OF PHOTON BUBBLES

In order to better understand the coupled photon bubble-Parker problem, it is useful to derive the properties of pure Parker modes in the absence of photon bubble instabilities. We are most interested in a medium where radiation pressure dominates gas pressure, and in short wavelengths where radiative diffusion is rapid. The latter condition implies that temperature perturbations are very small, and if we take them literally to be zero, then the flux perturbations that drive photon bubble instabilities in this regime will vanish identically, leaving only pure Parker modes.

Parker modes with rapid radiative diffusion were first studied by Gilman (1970), who argued that it was a good first order approximation to replace the perturbed energy equation (14) with the statement that the temperature perturbation δT vanishes.

The linearized perturbation equations that we presented in subsection 2.2 can be combined with the perturbed flux-freezing equation to give the total (gas plus radiation plus magnetic) pressure perturbation in two radiative diffusion limits. The first is the adiabatic limit of infinitely slow diffusion ($\kappa \rightarrow \infty$, $F \rightarrow 0$, κF finite), giving

$$\begin{aligned} \delta P_{\text{tot}} = & \rho \left(c_t^2 + v_A^2 - \frac{k_y^2 v_A^2}{\omega^2} c_t^2 \right) \tilde{\delta} \rho - \rho \left[\frac{c_t^2 N^2}{g} + v_A^2 \frac{d}{dz} \ln \left(\frac{B}{\rho} \right) \right] \xi_z \\ & + \rho \left(\frac{k_y^2 v_A^2}{\omega^2} \right) \left[\frac{c_t^2 N^2}{g} + v_A^2 \frac{d}{dz} \ln B \right] \xi_z, \end{aligned} \quad (\text{A1})$$

where $\xi_z = \int \delta v_z dt = i \delta v_z / \omega$ is the vertical component of the Lagrangian displacement vector. The second is the limit of sufficiently short wavelengths that diffusion is rapid enough ($\kappa \rightarrow 0$) to guarantee that the perturbations are isothermal ($\delta T \rightarrow 0$). This gives

$$\delta P_{\text{tot}} = \rho \left(c_i^2 + v_A^2 - \frac{k_y^2 v_A^2}{\omega^2} c_i^2 \right) \tilde{\delta} \rho - \rho v_A^2 \frac{d}{dz} \ln \left(\frac{B}{\rho} \right) \xi_z$$

$$+ \rho \left(\frac{k_y^2 v_A^2}{\omega^2} \right) \left[v_A^2 \frac{d}{dz} \ln B \right] \xi_z. \quad (\text{A2})$$

Equations (A1) and (A2) contain the essential physics of the Parker instability in both of these limits. Buoyancy is maximized for a vertically displaced fluid element if it is in pressure equilibrium with its surroundings, i.e. $\delta P_{\text{tot}} = 0$. Solving the resulting equation for the Eulerian density perturbation associated with an upward fluid element displacement ($\xi_z > 0$) then gives instability if $\tilde{\delta}\rho < 0$. There are two possibilities depending on k_y . For $k_y \rightarrow 0$, the first ξ_z term on the right hand sides of equations (A1) and (A2) dominates. In this case, the perturbation involves a straight bundle of field lines, and the resulting mode is called an interchange mode. On the other hand, for k_y sufficiently large, the second ξ_z term dominates, and the perturbation involves a bending of the field lines, resulting in the undulatory mode.

In the adiabatic limit, the instability criteria for these two modes (Newcomb 1961; Acheson 1979; Christodoulou et al. 2003) are therefore

$$\begin{aligned} \frac{-g}{c_t^2} \frac{d}{dz} \ln \left(\frac{B}{\rho} \right) &> \frac{N^2}{v_A^2} \quad \text{interchange} \\ \frac{-g}{c_t^2} \frac{d}{dz} \ln B &> \frac{N^2}{v_A^2} \quad \text{undulatory.} \end{aligned} \quad (\text{A3})$$

In the rapid diffusion limit, on the other hand, the instability criteria may be written as (Gilman 1970; Acheson 1979)

$$\begin{aligned} \frac{-g}{c_i^2} \frac{d}{dz} \ln \left(\frac{B}{\rho} \right) &> 0 \quad \text{interchange} \\ \frac{-g}{c_i^2} \frac{d}{dz} \ln B &> 0 \quad \text{undulatory.} \end{aligned} \quad (\text{A4})$$

These are easier to satisfy than the criteria (A3) because pressure and temperature equilibrium between the perturbations and their surroundings makes the fluid hydrodynamically neutrally buoyant.

We consider only the rapid diffusion limit from now on. Using equation (A2), the linearized continuity and horizontal momentum equations can be combined to express the density and total pressure perturbations entirely in terms of the vertical velocity perturbation:

$$\tilde{\delta}\rho = \frac{-i\omega}{k_\perp^2 c_i^2 - \omega^2 \frac{\omega^2 - k_\perp^2 v_A^2}{\omega^2 - k_y^2 v_A^2}} \left[\frac{\omega^2 - k_\perp^2 v_A^2}{\omega^2 - k_y^2 v_A^2} \frac{\delta v_z}{H_\rho} + \frac{k_\perp^2 v_A^2}{2\omega^2 H_{\text{mag}}} \delta v_z - \frac{d\delta v_z}{dz} \right] \quad (\text{A5})$$

and

$$\delta P_{\text{tot}} = \frac{-i\omega\rho}{k_\perp^2 c_i^2 - \omega^2 \frac{\omega^2 - k_\perp^2 v_A^2}{\omega^2 - k_y^2 v_A^2}} \left[\frac{c_i^2}{H_\rho} \delta v_z + \frac{v_A^2}{2H_{\text{mag}}} \delta v_z - \left(c_i^2 + v_A^2 - \frac{k_y^2 v_A^2}{\omega^2} c_i^2 \right) \frac{d\delta v_z}{dz} \right]. \quad (\text{A6})$$

Here $k_\perp \equiv (k_x^2 + k_y^2)^{1/2}$ is the magnitude of the horizontal wavenumber.

These expressions can then be combined with the linearized vertical momentum equation,

$$-i\omega\rho\delta v_z = -\frac{\partial\delta P_{\text{tot}}}{\partial z} - \rho\tilde{\delta}\rho g - \frac{ik_y^2}{\omega}\rho v_A^2 \delta v_z, \quad (\text{A7})$$

to give an exact linear ordinary differential equation for the vertical velocity perturbation. In his analysis of the Parker instability in the limit of rapid radiative diffusion, Gilman (1970) derived a simplified form of this differential equation by first assuming $k_x \rightarrow \infty$ with ω and k_y remaining finite. From the x -component of the linearized momentum equation,

$$-i\omega\rho\delta v_x = -ik_x\delta P_{\text{tot}} - \frac{ik_y^2}{\omega}\rho v_A^2 \delta v_x, \quad (\text{A8})$$

this guarantees that $\delta P_{\text{tot}} \rightarrow 0$, giving a maximum buoyant response and therefore a maximum Parker growth rate. However, here we will allow for the possibility that k_y/k_x is not necessarily small in magnitude as k_x gets large. This is because the Parker cutoff wavenumber $k_P = [g/(2c_i^2 H_{\text{mag}})]^{1/2}$ can be very large in a radiation dominated plasma, in which the isothermal sound speed in the gas alone c_i can be very small. (In contrast, in the adiabatic limit, the Parker cutoff wavenumber is comparable to the inverse scale height of the background medium.) Because a plasma whose thermal pressure is dominated by radiation is necessarily supported against gravity by radiation pressure and/or magnetic pressure gradients, the Parker cutoff wavenumber in the rapid diffusion limit can be much larger than the inverse scale height of the background. It therefore makes sense to consider the possibility of very large, as well as very small, k_y .

We therefore take $|\omega^2| \ll k_\perp^2 v_A^2$, but not necessarily much smaller than $k_y^2 v_A^2$. The first derivative term in equation (A5) is higher order than the other terms for short wavelengths, so the density perturbation becomes

$$\tilde{\delta\rho} \simeq \frac{-i\omega v_A^2 \delta v_z}{\omega^2(c_i^2 + v_A^2) - k_y^2 v_A^2 c_i^2} \left(\frac{\omega^2 - k_y^2 v_A^2}{2\omega^2 H_{\text{mag}}} - \frac{1}{H_\rho} \right). \quad (\text{A9})$$

For the total pressure perturbation in equation (A6), the first derivative term dominates, and

$$\delta P_{\text{tot}} \simeq \frac{i\rho(\omega^2 - k_y^2 v_A^2)}{\omega k_\perp^2} \frac{\partial \delta v_z}{\partial z} \quad (\text{A10})$$

Substituting into the vertical momentum equation, employing the short wavelength WKB approximation $\partial/\partial z \rightarrow ik_z$, and simplifying, we finally obtain the dispersion relation

$$\begin{aligned} (v_A^2 + c_i^2)\omega^4 - \left[k_y^2 v_A^2 (v_A^2 + 2c_i^2) + \frac{g v_A^2 k_\perp^2}{k^2} \left(\frac{1}{H_\rho} - \frac{1}{2H_{\text{mag}}} \right) \right] \omega^2 \\ + k_y^2 v_A^4 \left(k_y^2 c_i^2 - \frac{g k_\perp^2}{2H_{\text{mag}} k^2} \right) = 0, \end{aligned} \quad (\text{A11})$$

where $k \equiv (k_\perp^2 + k_z^2)^{1/2}$ is the total wavenumber magnitude of the perturbation. Apart from the generalization that k_y and k_z no longer need be considered small compared to k_x , this is identical to equation (14) of Gilman (1970).

If either of the instability criteria (A4) are satisfied, then all nonzero wavenumbers k_y less than $k_\perp k_P/k$ will be unstable, where, again, the characteristic Parker cut off wavenumber is defined by

$$k_P^2 \equiv \frac{g}{2c_i^2 H_{\text{mag}}}. \quad (\text{A12})$$

The maximum undulatory instability growth rate is given by

$$\gamma_{\text{max}}^2 = \frac{k_\perp^2 g}{k^2 v_A^2} \left[\frac{c_i}{H_\rho^{1/2}} - \left(\frac{c_i^2}{H_\rho} + \frac{v_A^2}{2H_{\text{mag}}} \right)^{1/2} \right]^2, \quad (\text{A13})$$

and occurs at a wavenumber k_0 given by

$$k_0^2 = \frac{k_\perp^2 g}{k^2 v_A^4} \left[\left(\frac{c_i^2}{H_\rho} + \frac{v_A^2}{2H_{\text{mag}}} \right)^{1/2} - \frac{c_i}{H_\rho^{1/2}} \right] \left[\frac{v_A^2 + c_i^2}{c_i H_\rho^{1/2}} - \left(\frac{c_i^2}{H_\rho} + \frac{v_A^2}{2H_{\text{mag}}} \right)^{1/2} \right]. \quad (\text{A14})$$

Assuming that the gas sound speed is much less than the Alfvén speed (the regime of interest for this paper), equations (A13) and (A14) become

$$\gamma_{\text{max}}^2 = \frac{k_\perp^2 g}{2H_{\text{mag}} k^2}, \quad (\text{A15})$$

and

$$k_0^2 = \frac{k_\perp^2 g}{k^2 v_A c_i (2H_{\text{mag}} H_\rho)^{1/2}}. \quad (\text{A16})$$

THE ZERO GAS PRESSURE LIMIT WITH ROTATION AND SHEAR

Here we generalize the zero gas pressure limit analysis of section 3 to include the effects of rotation and shear on the coupled Parker/photon bubble instability problem in a differentially rotating accretion disk. Because we are interested in short wavelength perturbations, we focus on a local comoving patch of the accretion disk, and employ the shearing box approximation (Goldreich & Lynden-Bell 1965; Hawley, Gammie & Balbus 1995). The fluid equations (1)-(6) remain the same, except for two modifications.

The first is the addition of the terms $-2\rho\Omega\hat{\mathbf{z}} \times \mathbf{v} + 2q\rho\Omega^2 x\hat{\mathbf{x}}$ to the right hand side of the momentum equation (2), which represent the combined effects of Coriolis, centrifugal, and radial gravitational forces on the flow. Here Ω is the angular velocity of the local patch of disk and q is a shear parameter, representing a variation of angular velocity with radius r of $\Omega \propto r^{-q}$ ($q = 3/2$ for Keplerian shear). We employ a Cartesian basis $(\hat{\mathbf{x}}, \hat{\mathbf{y}}, \hat{\mathbf{z}})$, with $\hat{\mathbf{x}}$ in the local radial direction, $\hat{\mathbf{y}}$ in the local azimuthal direction, and $\hat{\mathbf{z}}$ in the vertical direction just as in the static equilibrium studied in the main body of the paper. We continue to write the vertical gravitational acceleration as $\mathbf{g} = -g\hat{\mathbf{z}}$, with $g = \Omega^2 z$, the equilibrium radiation flux as $\mathbf{F} = F\hat{\mathbf{z}}$, and the equilibrium magnetic field as $\mathbf{B} = B(z)\hat{\mathbf{y}}$, i.e. a purely azimuthal magnetic field. The equilibrium state continues to be described by equations (7)-(9), but in addition there is now an azimuthal flow velocity of $\mathbf{v} = -q\Omega x\hat{\mathbf{y}}$.

The second modification concerns horizontal boundary conditions. In the static analysis, we considered a horizontally homogeneous equilibrium, and perturbations that were periodic in the horizontal direction ($\propto \exp[i(k_x x + k_y y)]$).

The shearing box has all fluid variables subject to shearing periodic boundary conditions in the radial direction (Hawley, Gammie & Balbus 1995). The standard way to treat this is to make a coordinate transformation: $x' = x$, $y' = y + q\Omega x t$, $z' = z$, and $t' = t$. Our perturbations can then be taken to have a horizontal dependence of the form $\exp[i(k_x(t')x + k_y y)]$, where the wavenumber in the x -direction is time-dependent:

$$k_x(t') = k_{x0} + q\Omega t' k_y \quad (\text{B1})$$

Here k_{x0} and k_y are independent of time. Horizontal derivatives acting on perturbations can therefore be written as $\partial/\partial x \rightarrow ik_x(t')$ and $\partial/\partial y \rightarrow ik_y$. We also adopt the Lagrangian time derivative operator

$$\frac{\partial}{\partial t'} = \frac{\partial}{\partial t} - q\Omega x \frac{\partial}{\partial y}. \quad (\text{B2})$$

The explicit time-dependence of the radial wavenumber implies that a Lagrangian treatment of the perturbation equations is much easier than an Eulerian treatment. We therefore work in terms of the Lagrangian displacement vector $\boldsymbol{\xi}$, which to linear order is related to the Eulerian velocity perturbation by

$$\delta \mathbf{v} = \frac{\partial \boldsymbol{\xi}}{\partial t'} + q\Omega \xi_x \hat{\mathbf{y}}. \quad (\text{B3})$$

This allows us to immediately solve the continuity and flux-freezing equations to express the Eulerian density and magnetic field perturbations in terms of the Lagrangian displacement (Newcomb 1962). To linear order,

$$\delta \rho = -i\rho k_x \xi_x - i\rho k_y \xi_y - \rho \frac{\partial \xi_z}{\partial z} - \xi_z \frac{d\rho}{dz}, \quad (\text{B4})$$

$$\delta B_x = ik_y B \xi_x, \quad (\text{B5})$$

$$\delta B_y = -\xi_z \frac{dB}{dz} - B \frac{\partial \xi_z}{\partial z} - iB k_x \xi_x, \quad (\text{B6})$$

and

$$\delta B_z = ik_y B \xi_z. \quad (\text{B7})$$

Eliminating the density and magnetic field perturbations, the linearized momentum equations are then

$$\frac{\partial^2 \xi_x}{\partial t'^2} = -i \frac{k_x}{\rho} \delta P - (k_x^2 + k_y^2) v_A^2 \xi_x + 2q\Omega^2 \xi_x + 2\Omega \frac{\partial \xi_y}{\partial t'} - i \frac{k_x v_A^2}{2H_{\text{mag}}} \xi_z + ik_x v_A^2 \frac{\partial \xi_z}{\partial z}, \quad (\text{B8})$$

$$\frac{\partial^2 \xi_y}{\partial t'^2} = -i \frac{k_y}{\rho} \delta P - 2\Omega \frac{\partial \xi_x}{\partial t'} - i \frac{k_y v_A^2}{2H_{\text{mag}}} \xi_z, \quad (\text{B9})$$

and

$$\begin{aligned} \frac{\partial^2 \xi_z}{\partial t'^2} = & -\frac{1}{\rho} \frac{\partial \delta P}{\partial z} - k_y^2 v_A^2 \xi_z + \frac{v_A^2}{(H'_{\text{mag}})^2} \xi_z - \frac{3v_A^2}{2H_{\text{mag}}} \frac{\partial \xi_z}{\partial z} + v_A^2 \frac{\partial^2 \xi_z}{\partial z^2} - i \frac{k_x v_A^2}{H_{\text{mag}}} \xi_x \\ & + ik_x v_A^2 \frac{\partial \xi_x}{\partial z} + igk_x \xi_x + igk_y \xi_y + g \frac{\partial \xi_z}{\partial z} - \frac{g}{H_\rho} \xi_z. \end{aligned} \quad (\text{B10})$$

The thermal pressure perturbation can be derived from the linearized energy equation. Assuming negligible gas pressure, and eliminating the flux perturbation using the radiation diffusion equation, this is

$$3 \frac{\partial \delta P}{\partial t'} + \delta v_z \frac{dE}{dz} + \frac{4}{3} E \nabla \cdot \delta \mathbf{v} = -F \frac{\partial \tilde{\delta} \rho}{\partial z} + \frac{c}{\kappa \rho H_\rho} \frac{\partial \delta P}{\partial z} + \frac{c}{\kappa \rho} (k_x^2 + k_y^2) \delta P + \frac{c}{\kappa \rho} \frac{\partial^2 \delta P}{\partial z^2}. \quad (\text{B11})$$

Thus far, all of our equations are exact in the zero gas pressure limit. We now employ the WKB approximation in z , assuming that all perturbations have a z -dependence of $\exp(ik_z z)$ and take all wavenumber components to be large. Because we are looking for instabilities with growth rates that increase with wavenumber no faster than $k^{1/2}$, the time derivative term in the energy equation is small. Physically, radiative diffusion is extremely fast at short wavelengths compared to our instability growth times, i.e. we are in the rapid diffusion limit. Eliminating the time derivative here eliminates the damped diffusion mode of equation (19). The remaining terms with the largest dependence on wavenumber then allow us to approximate the thermal pressure perturbation as

$$\delta P \simeq \frac{\kappa \rho}{ck^2} \left[F k_z (k_x \xi_x + k_y \xi_y + k_z \xi_z) - \frac{4E}{3} \left(ik_x \frac{\partial \xi_x}{\partial t'} + ik_y \frac{\partial \xi_y}{\partial t'} + ik_z \frac{\partial \xi_z}{\partial t'} + ik_y q \Omega \xi_x \right) \right]. \quad (\text{B12})$$

The momentum equations can also be simplified by first noting that the second order time derivative terms on the left hand sides of equations (B8) and (B10) are negligible given the $\sim k^2$ magnetic force terms on the right hand sides. Physically, eliminating these time derivatives eliminates the fast and Alfvén modes of equations (20) and

(21). Equations (B8) and (B10) can then be used to eliminate ξ_x and ξ_z from equation (B9). The algebra is greatly simplified if one first recognizes that in this limit of negligible gas pressure, slow modes have fluid displacements that are predominately along the magnetic field (in the y -direction). In fact, ξ_x and ξ_z are one power of k smaller than ξ_y . Keeping only the lowest order terms as $k \rightarrow \infty$, and assuming that magnetic gradients dominate radiation pressure gradients in supporting the equilibrium (so that $k_{\text{tran}} H_{\text{mag}} \gg 1$ and the Parker regime generally exists in the WKB limit for all wavenumber orientations), we finally obtain the following differential equation:

$$\frac{\partial^2 \xi_y}{\partial t'^2} + \frac{k_y^2}{k^2} \frac{4E\kappa}{3c} \frac{\partial \xi_y}{\partial t'} - \frac{(k_x^2 + k_y^2)v_A^2}{4H_{\text{mag}}^2 k^2} \xi_y + i \frac{k_y^2 k_z}{k^2} \frac{\kappa F}{c} \xi_y = 0. \quad (\text{B13})$$

If there were no shear ($q = 0$), so that the radial wavenumber k_x was independent of time, we could assume a complex exponential time-dependence $\xi_y \propto \exp(-i\omega t')$ and recover the static equilibrium dispersion relation (27).

The Coriolis accelerations are simply too small to have affected the modes at short wavelengths. To order of magnitude, assuming a typical Parker growth rate $\sim v_A/H_{\text{mag}}$, the Coriolis terms in equations (B8) and (B9) are negligible provided $\Omega \ll kv_A$. But for a magnetically supported equilibrium, $\Omega \sim v_A/H_{\text{mag}}$, so this is just equivalent to the WKB condition $kH_{\text{mag}} \gg 1$. In more detail, we require $|k_z|H_{\text{mag}} \gg k|k_y|/(|k_x|k_\perp)$, so that large radial wavenumbers better ensure immunity of the Parker instability from Coriolis effects (Shu 1974). Provided $k_{\text{tran}} H_{\text{mag}} \gg 1$, the photon bubble regime will be even less affected by Coriolis forces.

REFERENCES

- Acheson, D. J. 1979, *Solar Phys.*, 62, 23
Arons, J. 1992, *ApJ*, 388, 561
Begelman, M. C. 2001, *ApJ*, 551, 897
Begelman, M. C. 2002, *ApJ*, 568, 97
Begelman, M. C. 2006a, *ApJ*, 636, 995
Begelman, M. C. 2006b, *ApJ*, 643, 1065
Blaes, O., Hirose, S., & Krolik, J. H. 2007, *ApJ*, 664, 1057
Blaes, O., Krolik, J. H., Hirose, S., & Shabaltas, N. 2011, *ApJ*, 733, 110
Blaes, O., & Socrates, A. 2001, *ApJ*, 553, 987
Blaes, O., & Socrates, A. 2003, *ApJ*, 596, 509
Chandrasekhar, S. 1967, *An Introduction to the Study of Stellar Structure* (New York: Dover)
Christodoulou, D. M., Contopoulos, J., & Kazanas, D. 2003, *ApJ*, 586, 372
Gammie, C. F. 1998, *MNRAS*, 297, 929
Gilman, P. A. 1970, *ApJ*, 162, 1019
Goldreich, P., & Lynden-Bell, D. 1965, *MNRAS*, 130, 125
Hawley, J. F., Gammie, C. F., & Balbus, S. A. 1995, *ApJ*, 440, 742
Hirose, S., Krolik, J. H., & Blaes, O. 2009, *ApJ*, 691, 16
Krolik, J. H., Hirose, S., & Blaes, O. 2007, *ApJ*, 664, 1045
Miller, K. A., & Stone, J. M. 2000, *ApJ*, 534, 398
Newcomb, W. A. 1961, *Phys. Fluids*, 4, 391
Newcomb, W. A. 1962, *Nuclear Fusion Supplement*, 2, 451
Parker, E. N. 1966 *ApJ*, 145, 811
Parker, E. N. 1967, *ApJ*, 149, 535
Shu, F. H. 1974, *A&A*, 33, 55
Socrates, A., Blaes, O., Hungerford, A., & Fryer, C. L. 2005, *ApJ*, 632, 531
Socrates, A., Parrish, I. J., & Stone, J. M. 2008, *ApJ*, 675, 357
Stone, J. M., Mihalas, D., & Norman, M. L. 1992, *ApJS*, 80, 819
Tserkovnikov, Yu. A. 1960, *Soviet Phys. Dokl.*, 5, 87
Turner, N. J., Blaes, O. M., Socrates, A., Begelman, M. C., & Davis, S. W. 2005, *ApJ*, 624, 267